Strain-induced large spin splitting and persistent spin helix at LaAlO3/SrTiO3 interface

メタデータ	言語: eng
	出版者:
	公開日: 2021-07-02
	キーワード (Ja):
	キーワード (En):
	作成者:
	メールアドレス:
	所属:
URL	https://doi.org/10.24517/00062822

Strain-induced large spin splitting and persistent spin helix at LaAlO$_3$/SrTiO$_3$ interface

Naoya Yamaguchi[1] [*] and Fumiyuki Ishii[2] [†]

[1] *Division of Mathematical and Physical Sciences, Graduate School of Natural Science and Technology, Kanazawa University, Kanazawa, 920-1192, Japan.*
[2] *Faculty of Mathematics and Physics, Institute of Science and Engineering, Kanazawa University, Kanazawa, 920-1192, Japan.*

We investigated the effect of the tensile strain on the spin splitting at the n-type interface in LaAlO$_3$/SrTiO$_3$ in terms of the spin-orbit coupling coefficient α and spin texture in the momentum space using first-principles density functional calculations. We found that the α could be controlled by the tensile strain and be enhanced up to 5 times for the tensile strain of 7%, and the effect of the tensile strain leads to a persistent spin helix, which has a long spin lifetime. The strain effect on LaAlO$_3$/SrTiO$_3$ is important for various applications such as spin field-effect transistor and spin-to-charge conversion.

The LaAlO$_3$/SrTiO$_3$ interface is one of the most important heterostructures, which has an n-type interface with high mobility two-dimensional electronic gas (2DEG).[1,2] Recently, Rashba effect in LaAlO$_3$/SrTiO$_3$ has attracted much attention due to potential applications in spintronics.[3] For example, spin-to-charge conversion phenomenon induced by the inverse Rashba–Edelstein effect (IREE) for LaAlO$_3$/SrTiO$_3$ was reported.[4] IREE can be used for an alternative mechanism of detection of spin current utilizing inverse spin Hall effect,[5] and it is suggested that the strength of the IREE was proportional to the Rashba coefficient α_R.[6] Therefore it is quite important to control the Rashba effect at the LaAlO$_3$/SrTiO$_3$ interface.

The applied electric field can control the magnitude of α_R. The α_R in LaAlO$_3$/SrTiO$_3$ induced by built-in electric field was experimentally evaluated as 18 meV·Å and it was increased up to 49 meV·Å by applying electric field.[3] In epitaxial oxide thin films and superlattices, strain induced by substrates, is useful to control electronic structures and physical properties, and so important that its effects are extensively studied for various materials.[7] Some works about the strain for LaAlO$_3$/SrTiO$_3$ actually were reported.[8,9] Bulk SrTiO$_3$ shows strain-induced ferroelectric phase transition,[10] and the electric polarization is induced

by the tensile strain along the [110]-direction. Since the 2DEG at the n-type interface in LaAlO$_3$/SrTiO$_3$ may be influenced by the strain-induced electric polarization, the spin splitting, especially spin-orbit coupling coefficient α, can be controlled by the strain. In fact, a first-principles calculation of strain control of the Rashba spin splitting in ZnO was reported.[11]

In this work, we focus the spin splitting at the n-type interface in LaAlO$_3$/SrTiO$_3$, and investigate the effect of tensile strain on it in terms of the spin-orbit coupling coefficient α and spin texture using first-principles calculations. We found that the α could be controlled by the tensile strain and be enhanced up to 5 times for the tensile strain of 7%, and the effect of the tensile strain leads to a persistent spin helix, which has a long spin lifetime. These properties are expected to be important to various spintronic applications.

Rashba effect[12] arises from spin-orbit interaction for the 2DEG at the surfaces and interfaces with the spatial inversion symmetry breaking, and the Hamiltonian describing Rashba effect in the 2DEG can be expressed by $H = -\hbar^2 \nabla_\parallel^2/(2m^*) + H_R$, where $\hbar$ is the Planck constant, and m^* is the effective mass of electrons. The Rashba Hamiltonian: $H_R = \alpha_R(\hat{e}_z \times \vec{k}_\parallel) \cdot \vec{\sigma} = \alpha_R(k_y \sigma_x - k_x \sigma_y)$, where α_R denotes the Rashba coefficient, $\hat{e}_z$ the unit vector along z-axis, $\vec{k}_\parallel = (k_x, k_y, 0)$ the wave vector, and $\vec{\sigma} = (\sigma_x, \sigma_y, \sigma_z)$ the Pauli matrices vector, respectively. We can obtain the energy dispersion relation: $E_\pm(\vec{k}_\parallel) = \hbar^2 k_\parallel^2/(2m^*) \pm \alpha_R k_\parallel$. The α_R satisfies $\alpha_R = 2E_R/k_R$, where E_R ($= m^* \alpha_R^2/(2\hbar^2)$) is the Rashba energy, and k_R ($= m^* \alpha_R/\hbar^2$) the Rashba momentum offset.

For the interfacial system with the tensile strain in LaAlO$_3$/SrTiO$_3$, due to the strain-induced electric polarization along the [110]-direction originating from bulk SrTiO$_3$, there is expected to be only one mirror plane along the ($\bar{1}$10) plane. Indeed, we confirm that atomic displacement is induced along the ($\bar{1}$10) plane in atomic structures optimized by the first-principles calculation. Thus, the spin-orbit Hamiltonian can be expressed as $H_{SO} = \alpha_{xy}^\parallel k_x \sigma_y + \alpha_{yx}^\parallel k_y \sigma_x + \alpha_{[1\bar{1}0]z}^\perp \left(\frac{k_x - k_y}{\sqrt{2}}\right)\sigma_z$ in the same way as the analysis in the previous work of a ZnO (10$\bar{1}$0) surface with a mirror plane along the (100) plane.[13] While the $\alpha_{xy}^\parallel$ and $\alpha_{yx}^\parallel$ are corresponding to the Rashba effect, the $\alpha_{[1\bar{1}0]z}^\perp$ originates from the strain-induced electric polarization. As the tensile strain increases, $H_{[1\bar{1}0]z}^\perp = \alpha_{[1\bar{1}0]z}^\perp \left(\frac{k_x - k_y}{\sqrt{2}}\right)\sigma_z$ is expected to be more dominant. The spin texture for $H_{[1\bar{1}0]z}^\perp$ has the spin splitting along the [1$\bar{1}$0]-direction, and the $\alpha_{[1\bar{1}0]z}^\perp$ can be evaluated in the same way as α_R for the Rashba system: $\alpha_{[1\bar{1}0]z}^\perp = 2E_{[1\bar{1}0]z}^\perp/k_{[1\bar{1}0]z}^\perp$. We take the α_R and $\alpha_{[1\bar{1}0]z}^\perp$ as $\alpha_{[1\bar{1}0]}$ hereafter.

We perform density functional calculations using the computational model of the superlattice (LaAlO$_3$)$_6$/(SrTiO$_3$)$_6$ shown in Fig. 1(a), where the n-type interface indicates the one
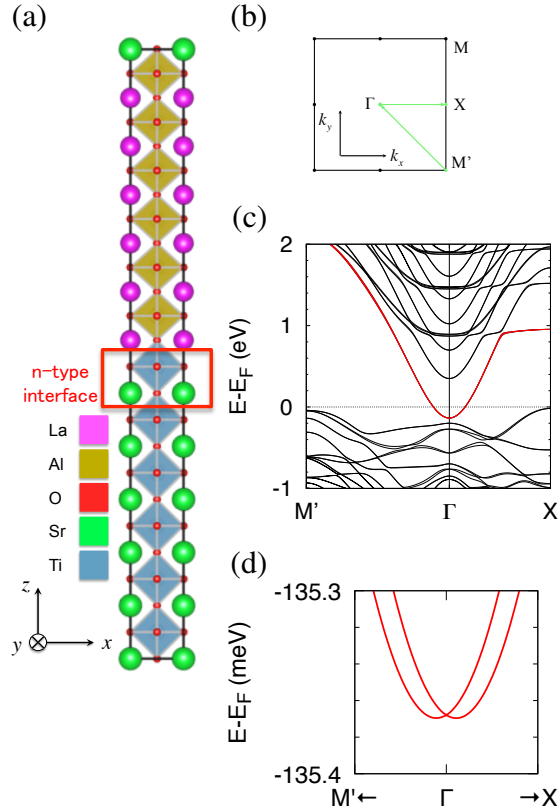
Fig. 1. : (a) Computational model. (b) Schematic of the first Brillouin zone. (c) Band structure for unstrained LaAlO$_3$/SrTiO$_3$. The red curves show the bands with the Rashba spin splitting. (d) Enlarged view for the interfacial bands around Γ-point.

between the TiO$_2$ and LaO layers. It was suggested that the number of the formula unit of LaAlO$_3$ or SrTiO$_3$ was required to be 6 to describe the metallic ground state with atomic relaxation.[14–17] We use the experimental lattice constants: a_0^{LAO}=3.788 Å[18] for LaAlO$_3$; a_0^{STO}=3.905 Å[19] for SrTiO$_3$, and the supercell length c is determined with the cell volume conserved. We assumed the biaxial misfit strain $(a - a_0^{STO})/a$, where a denotes the in-plane lattice constant (xy-plane), and the positive strain is tensile. Our calculations are performed within the general gradient approximation[20] by OpenMX code,[21] with the fully relativistic total angular momentum dependent pseudopotentials taking spin-orbit interaction (SOI) into account.[22] We adopt norm-conserving pseudopotentials with an energy cutoff of 300 Ry for charge density including the 5s, 5p, 5d and 6s-states as valence states for La; 3s and 3p for Al; 2s and 2p for O; 4s, 4p and 5s for Sr; 3s, 3p, 3d and 4s for Ti. We use $8 \times 8 \times 1$ regular k-point mesh. The numerical pseudo atomic orbitals are used as follows: the numbers of the s-, p-, d- and f-character orbitals are 3, 3, 1 and 1, respectively, for La; 3, 3, 1 and 0 for Al and O; 3, 2, 1 and 0 for Sr; 3, 3, 2 and 0 for Ti. The cutoff radii of La, Al, O, Sr and Ti are 6.0, 7.0, 5.0, 10.0 and 7.0, respectively, in units of Bohr.
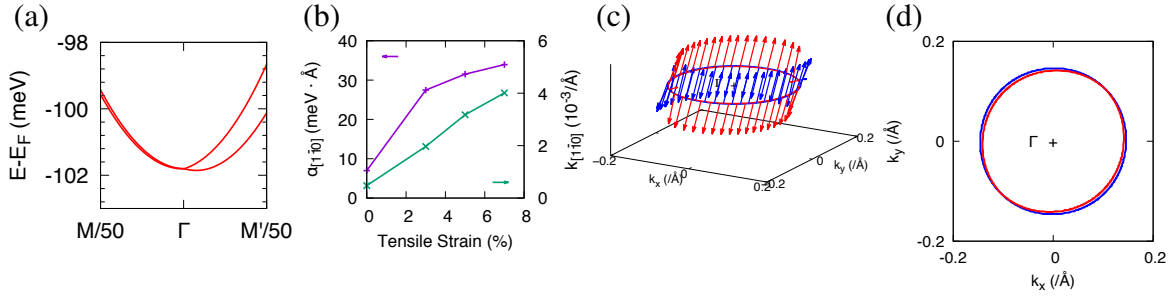
Fig. 2. : (a) Enlarged view for the interfacial bands about the spin splitting at the tensile strain of 5%. (b) Strain dependence for the spin-orbit coefficient $\alpha_{[1\bar{1}0]}$ and the momentum offset $k_{[1\bar{1}0]}$. (c) Spin textures at the tensile strain of 5%. (d) Fermi arcs at the tensile strain of 5%.

The calculated band structure for the unstrained system is shown in Fig. 1(c), and Fig. 1(d) is the enlarged view of the interfacial bands that we focus on. Analyzing the partial density of states (PDOS), we confirm that the interfacial band, that is, the conduction band edge (CBE) in the n-type interface mainly consist of the $3d_{xy}$ orbital as reported in the previous study.[23] For the tensile strain, the CBE is below the Fermi level so that the interface is metallic. This implies that the 2DEG remains for the tensile strain.

We calculate the spin-orbit coupling coefficient $\alpha_{[1\bar{1}0]}$ along the [1$\bar{1}$0]-direction (Γ to M') at the n-type interface for the spin splitting under the tensile strain inducing the 2DEG. With the tensile strain, we find larger spin splitting compared to the unstrained system as shown in Fig. 2(a). Figure 2(b) shows the strain dependence for the $\alpha_{[1\bar{1}0]}$ and the momentum off-set $k_{[1\bar{1}0]}$ for the interfacial bands around Γ-point. Without strain, our calculated $\alpha_{[1\bar{1}0]}$ (7.49 meV·Å) is of the same order as the prior works (18 meV·Å (expt.);[3] 12.6 meV·Å (theor.)[17]). As the tensile strain increases, the magnitude of the $\alpha_{[1\bar{1}0]}$ increases. The strain-induced electric polarization along the [110]-direction (Γ to M) may enhance the polarity, which makes $\alpha_{[1\bar{1}0]}$ larger. The strain-induced ferroelectricity was reported at room temperature,[10] where the electric polarization is somewhat weaker than at zero temperature, which corresponds to our result. The $\alpha_{[1\bar{1}0]}$, that is, spin splitting can be controlled by the tensile strain to get the about 5 times larger $\alpha_{[1\bar{1}0]}$ for the tensile strain of 7%. The spin textures in the strained system may be effective for IREE since the inner and outer Fermi arcs show the opposite spin textures (See Figs. 2(c) and 2(d)) so that the spin accumulation process may shift each Fermi arc to the opposite side, while the spin splitting is not Rashba-type one. There is a relation between the spin splitting and IREE length λ_{IREE}, correspondng to the efficiency of spin-to-charge conversion: $\lambda_{IREE} = j_c/j_s = \alpha_R\tau_s/\hbar$,[6] where j_c is the interfacial charge current density, j_s the spin current density, and τ_s the spin relaxation time. In the strained system, the magnitude of
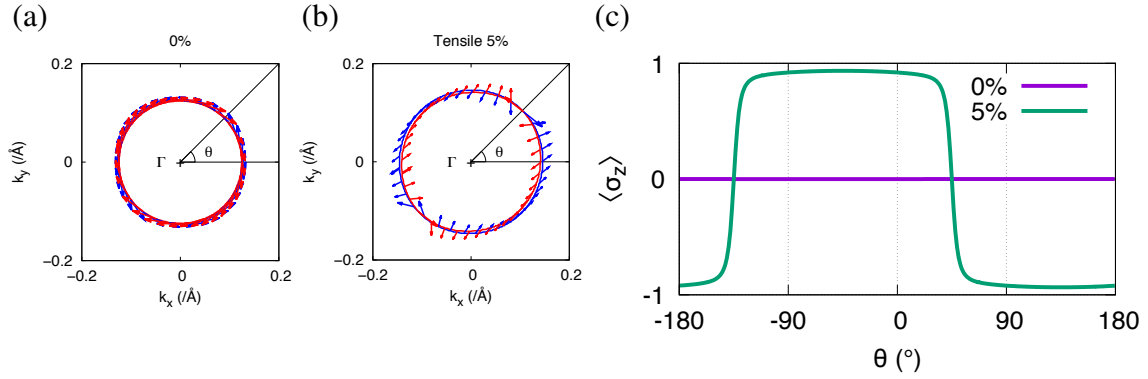
Fig. 3. : (a), (b): In-plane spin textures for the Rashba spin splitting at the Fermi level for each strain: (a) 0%; (b) Tensile 5%. The blue (red) arrow shows the expectation values of in-plane components of the Pauli matrices vector for the outer (inner) Fermi arc. (c): Angular dependence for the expectation value of the out-of-plane component σ_z of the Pauli matrices vector in the outer Fermi arc for each strain. θ is measured anticlockwise and defined as an angle in the polar coordinate system where its reference point is Γ-point and reference direction is the [100]-direction (Γ to X).

the $\alpha_{[1\bar{1}0]}$, instead of α_R, can be considered to be directly connected to λ_{IREE}. The effect of the tensile strain may enhance the λ_{IREE} in LaAlO$_3$/SrTiO$_3$ due to the larger α.[4]

In order to obtain the information of the spin-orbit Hamiltonian inducing the spin splitting, we calculate spin textures shown in Fig. 3. For the unstrained case (0%), our calculated spin texture shown in Fig. 3(a) shows a typical Rashba spin splitting, which is an agreement with the previous study.[17] As the tensile strain increases, however, the nature of the spin texture changes dramatically. For the tensile strain (See Figs. 2(c), 3(b) and 3(c)), the spin texture is different from the Rashba-type one, and also has the nonzero out-of-plane component that can be considered to originate from the spin-orbit Hamiltonian $H^\perp_{[1\bar{1}0]z} = \alpha^\perp_{[1\bar{1}0]z} \left(\frac{k_x - k_y}{\sqrt{2}} \right) \sigma_z$. In this case, the out-of-plane (σ_z) component is almost constant for the k-points except part of the Fermi arc around the degenerate points in the [110]-direction ($\theta = 45°, -135°$) so that the electronic states may have a long spin lifetime. This suggests that the persistent spin helix (PSH)[13,24–26] may be formed. PSH has one-dimensionally-oriented spin components inducing a long spin lifetime.[24] The 2DEG in strained LaAlO$_3$/SrTiO$_3$, therefore, has a long spin relaxation time, compared to the previous works,[27–29] so that the greatly larger spin-to-charge conversion may be realized. The estimated PSH period λ_{PSH} is $\pi/k_{[1\bar{1}0]} = 0.098~\mu m$, which is comparable with that for a ZnO (10$\bar{1}$0) surface (0.19 μm),[13] and is two order of magnitude smaller than that for a GaAs/AlGaAs quantum well (7.3-10 μm).[26] Therefore, the PSH state of strained LaAlO$_3$/SrTiO$_3$ is suitable for miniaturization of spintronic devices such as spin field-effect transistor (spinFET).[30]

In summary, we have performed first-principles density functional calculations for the

n-type interface in $LaAlO_3/SrTiO_3$ with the tensile strain. We found that the spin-orbit coupling coefficient α directly connected to IREE could be controlled by the tensile strain and enhanced up to 5 times for the tensile strain of 7%. The PSH may be induced for the tensile strain so that the extremely long spin lifetime can be achieved. Moreover, the estimated PSH period λ_{PSH} is comparable with that for a ZnO ($10\bar{1}0$) surface and is also two order of magnitude smaller than that for a GaAs/AlGaAs quantum well.[26] The 2DEG in oxide surfaces[31,32] and interfaces[33] may be a promising candidate for miniaturization of spintronic devices utilizing PSH. These results support that the strain effect in $LaAlO_3/SrTiO_3$ is important for various applications such as spinFET and spin-to-charge conversion.

Acknowledgment

References

1) A. Ohtomo and H. Hwang: Nature **427**, 423 (2004).

2) S. Thiel: Science **313**, 1942 (2006).

3) A. Caviglia, M. Gabay, S. Gariglio, N. Reyren, C. Cancellieri and J. Triscone: Phys. Rev. Lett. **104**, 126803 (2010).

4) E. Lesne, Y. Fu, S. Oyarzun, R. JC, D. Vaz, H. Naganuma, G. Sicoli, J. Attané, M. Jamet, E. Jacquet, J. George, A. Barthélémy, H. Jaffrès, A. Fert, M. Bibes and L. Vila: Nat. Mater. **15**, 1261 (2016).

5) E. Saitoh, M. Ueda, H. Miyajima and G. Tatara: Appl. Phys. Lett. **88**, 182509 (2006).

6) R. J. Sánchez, L. Vila, G. Desfonds, S. Gambarelli, J. Attané, D. J. Teresa, C. Magén and A. Fert: Nat. Commun. **4**, 2944 (2013).

7) O. Diéguez, K. Rabe and D. Vanderbilt: Phys. Rev. B **72**, 144101 (2005).

8) C. Bark, D. Felker, Y. Wang, Y. Zhang, H. Jang, C. Folkman, J. Park, S. Baek, H. Zhou, D. Fong, X. Pan, E. Tsymbal, M. Rzchowski and C. Eom: Proc. Natl. Acad. Sci. **108**, 4720 (2011).

9) D. Doennig and R. Pentcheva: Sci. Reports. **5**, 7909 (2015).

10) J. Haeni, P. Irvin, W. Chang, R. Uecker, P. Reiche, Y. Li, S. Choudhury, W. Tian, M. Hawley, B. Craigo, A. Tagantsev, X. Pan, S. Streiffer, L. Chen, S. Kirchoefer, J. Levy and D. Schlom: Nature **430**, 758 (2004).

11) M. Absor, H. Kotaka, F. Ishii and M. Saito: Appl. Phys. Express **7**, 053002 (2014).

12) Y. A. Bychkov and E. I. Rashba: JETP Lett. **39**, 78 (1984).

13) M. Absor, F. Ishii, H. Kotaka and M. Saito: Appl. Phys. Express **8**, 073006 (2015).

14) S. Ishibashi and K. Terakura: J. Phys. Soc. Jpn. **77**, 104706 (2008).

15) M. Park, S. Rhim and A. J. Freeman: Phys. Rev. B **74**, 205416 (2006).

16) R. Pentcheva and W. E. Pickett: Phys. Rev. Lett. **102**, 107602 (2009).

17) M. Nishida, F. Ishii, H. Kotaka and M. Saito: Mol. Simulat. **41**, 923 (2014).

18) V. Savchenko, L. Ivashkevich and V. Meleshko: Inorg. Mater. **21**, 1499 (1985).

19) Y. Inaguma, J. Sohn, I. Kim, M. Itoh and T. Nakamura: J. Phys. Soc. Jpn. **61**, 3831 (1992).

20) J. Perdew, K. Burke and M. Ernzerhof: Phys. Rev. Lett. **77**, 3865 (1996).

21) OpenMX: Open source package for Material eXplorer. http://www.openmx-square.org.

22) G. Theurich and N. A. Hill: Phys. Rev. B **64**, 073106 (2001).

23) Y. Du, C. Wang, J. Li, X. Zhang, F. Wang, Y. Zhu, N. Yin and L. Mei: Comput. Mater.

Sci. **99**, 57 (2015).

24) B. Bernevig, J. Orenstein and S. Zhang: Phys. Rev. Lett. **97**, 236601 (2006).

25) J. Koralek, C. Weber, J. Orenstein, B. Bernevig, S. Zhang, S. Mack and D. Awschalom: Nature **458**, 610 (2009).

26) M. Walser, C. Reichl, W. Wegscheider and G. Salis: Nat. Phys. **8**, 757 (2012).

27) C. Sahin, G. Vignale and M. Flatté: Phys. Rev. B **89**, 155402 (2014).

28) R. Ohshima, Y. Ando, K. Matsuzaki, T. Susaki, M. Weiler, S. Klingler, H. Huebl, E. Shikoh, T. Shinjo, S. T. Goennenwein and M. Shiraishi: Nat. Mater. **16**, 609 (2017).

29) M. Jin, S. Moon, J. Park, V. Modepalli, J. Jo, S. Kim, H. Koo, B. Min, H. Lee, S. Baek and J. Yoo: Nano Lett. **17**, 36 (2017).

30) S. Datta and B. Das: Appl. Phys. Lett. **56**, 665 (1990).

31) S. A., O. Copie, T. Kondo, F. Fortuna, S. Pailhès, R. Weht, X. Qiu, F. Bertran, A. Nicolaou, T. A., P. Fèvre, G. Herranz, M. Bibes, N. Reyren, Y. Apertet, P. Lecoeur, A. Barthélémy and M. Rozenberg: Nature **469**, 189 (2011).

32) P. King, R. He, T. Eknapakul, P. Buaphet, S. Mo, Y. Kaneko, S. Harashima, Y. Hikita, M. Bahramy, C. Bell, Z. Hussain, Y. Tokura, Z. Shen, H. Hwang, F. Baumberger and W. Meevasana: Phys. Rev. Lett. **108**, 117602 (2012).

33) K. Yang, S. Nazir, M. Behtash and J. Cheng: Sci. Reports **6**, 34667 (2016).